UCRL-JC-121280
Preprint

Three-Dimensional Simulations of High-Current Beams in Induction Accelerators with WARP3D

D.P. Grote, A. Friedman
I. Haber, S. Yu

This paper was prepared for submittal to the
International Symposium on Heavy Ion Fusion
Princeton, NJ
September 6-9, 1995

September 1, 1995

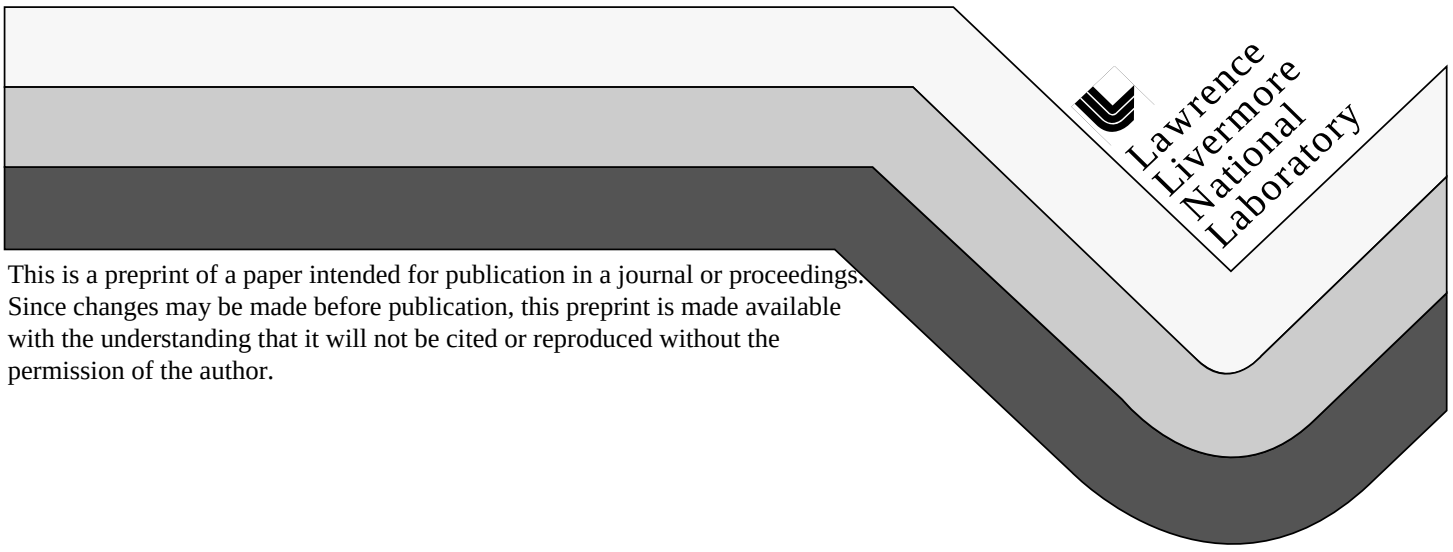

THREE-DIMENSIONAL SIMULATIONS OF HIGH-CURRENT BEAMS IN INDUCTION ACCELERATORS WITH WARP3d *

David P. Grote and Alex Friedman
Lawrence Livermore National Laboratory
Livermore, CA 94550 USA

Irving Haber
Naval Research Laboratory
Washington DC 20375-5346 USA

Simon Yu
Lawrence Berkeley National Laboratory, Berkeley, CA USA

For many issues relevant to acceleration and propagation of heavy-ion beams for inertial confinement fusion, understanding the behavior of the beam requires the self-consistent inclusion of the self-fields of the beams in multiple dimensions. For these reasons, the three-dimensional simulation code WARP3d A.Friedman[1] was developed. The code combines the particle-in-cell plasma simulation technique with a realistic description of the elements which make up an accelerator. In this paper, the general structure of the code is reviewed and details of two ongoing applications are presented along with a discussion of simulation techniques used. The most important results of this work are presented.

1. Introduction

The realization of heavy ion driven inertial fusion requires a detailed quantitative understanding of the behavior of high-current ion beams. The WARP3d code is used to study the transport and acceleration of space-charge dominated ion beams in present-day and near-term experiments, and in fusion drivers. In the two applications presented and in a number of others, WARP3d has proven to be an effective tool in understanding high-current beam dynamics.

The first application presented is the novel electrostatic quadrupole injector experiment at LBNL. WARP3d has played a major role in developing our understanding of how the nonlinear fields from the quadrupole geometry affect the beam behavior. Comparisons are made between simulations and experimental results. Both steady-state and time-dependent injection have been examined, the latter using a space-charge limited injection model.

The second application is multi-lap operation of a prototype recirculating induction accelerator. The primary concern of the simulations has been the effect of the electric dipole bending plates on the beam. The geometry of the plate conductors and the surrounding

* Work performed under auspices of U.S. DoE by LLNL, NRL, and LBNL under contracts W-7405-ENG-48, DE-AI02-93ER40799, DE-AI02-94ER54232, and DE-AC03-765F00098.

walls is included in the simulations. Using a plate design developed with WARP3d, a simulated beam has been successfully accelerated over 15 laps with little growth in the emittance.

2. WARP3d Overview

The WARP3d code combines the particle-in-cell plasma simulation technique with a realistic description of the elements which make up an accelerator. The code's accelerator "lattice" consists of a fully general set of focusing and bending elements. These elements are described in the laboratory frame. The lattice can be periodic. The description includes the strengths of the fields, location of the elements, and other properties specific to the types of elements. For flexibility, each multipole component is specified separately–this allows the possibility of overlapping elements. The lattice fields are calculated in the local laboratory frame for each particle at each time step. These fields, along with the self-consistently calculated self-fields, are used in the Lorentz force law to advance the particles at each time step. For efficiency, the lattice information is loaded onto a one-dimensional local grid which moves with the beam at the beginning of each time step. This avoids having to search the master list to find the information for each particle.

The code's particle-in-cell sections calculate particle trajectories and self-consistent electrostatic fields from the particles' positions. The particle trajectories are calculated with the leapfrog advance, using either full steps for efficiency or split steps to leave the particle's velocity and position synchronized in time for diagnostics. Residence corrections are used to account for differing number of steps through sharp-edged elements; without residence corrections, particles landing inside an element a differing number of times would receive dramatically different impulses. The self-potential ϕ is calculated via a Poisson solver on a co-moving mesh that is only slightly larger than the beam. The electric fields are applied by directly differencing ϕ for each particle.

In a bend, each particle is described in its own Cartesian frame; as the particle advances around the bend, the frame changes. Assuming a small inverse-aspect-ratio, an approximate algorithm is used. The dipole or bend field is augmented with a "pseudo-gyrofrequency" that accounts for the rate of change of the velocity angle due to the frame transformation. The algorithm is inexact since it does not account for the changes in beam position and velocity during the time step. The self-potential is calculated assuming a gentle bend. It is first calculated in Cartesian coordinates and then modified through iterations to include the non-Cartesian terms.

WARP3d includes a number of additional novel techniques and capabilities that both enhance its performance and make it applicable to a wider range of problems. The techniques include a method for subgrid scale resolution of conducting boundary locations in the solution of Poisson's equation, quasi-time dependent simulations for the efficient determination of equilibrium solutions, and the inclusion of externally or pre-calculated potentials. The capabilities include the ability to model the time-dependent accelerator gap fields used for axial beam confinement and compression, application of field multipole components as a function of axial location, or along with the residence correction for hard-edged elements, and multi-species beams. WARP3d is built on top of the Basis P.Dubois[2] system which allows interactive (run time) control of the code and access to

its internal database.

3. ESQ Injector

The electrostatic quadrupole (ESQ) injector experiment at LBNL S.Yu[3] S.Yu[4] E.Henestroza[5] will be the injector for the Elise experiment E.Lee[6], also at LBNL. The injector is required to supply 0.8 Ampere of 2 MeV singly-charged potassium ions at low normalized transverse emittance, less than 1 π-mm-mrad. The injector uses ESQ's (electrostatic quadrupoles) arranged to give a net acceleration along the axis while maintaining alternating gradient focusing. Figure 1 shows the layout of the injector with a beam filling the diode. A major issue is emittance growth from both the nonlinear multipole components of the focusing fields and the so-called "energy effect." The energy effect is the difference in axial velocity of particles on- and off-axis in an electrostatic element caused by the transverse variation of the potential. This effect is present in all electrostatic focusing systems and is generally insignificant, since the focusing potentials are a small fraction of the beam energy. However, at the low energy end of an ESQ injector, the focusing potential is about half of the beam energy.

3.1 Steady state behavior

For design of the lens optics only steady-state phenomena are of interest, so the runs were made in a quasi-time dependent fashion. The time step over which the fields were calculated is larger than the time step of the particle advance. The steady-state behavior is obtained after slightly more then one ion transit time across the injector. With this, simulation of a single quadrant, and subgrid-scale placement of the conductor boundaries, the three-dimensional simulations of the full injector required less than three minutes on a single processor of a Cray C-90, allowing the code to be used as a design tool.

The dimensions of the field grid, including the conductors, were typically 50×50 in the transverse directions and between 200 and 600 in the axial direction, depending on the number of quadrupoles in the system. The lengths of the runs were between 300 and 1000 time steps, again depending on the number of quadrupoles. From 70,000 to 300,000 particles were used.

The initial design was done using an envelope code that did not include the energy effect. The WARP3d simulations of that design showed significant emittance growth, up to 2 π-mm-mrad. By artificially canceling various multipole components in the simulations, it was found that about half of the emittance growth was the result of the V_{42} potential component ($\phi_{42} = V_{42} r^4 \cos 2\theta$).

The analytic solution of the single-particle motion shows that the energy effect acts as a fourth-order potential ($\phi \sim r^4$) which could be counteracted in the simulations by artificially applying additional fourth-order components. That showed that the energy effect accounted for the other half of the emittance growth. When the correction to the energy effect was applied and the V_{42} field was canceled, the beam experienced no observable emittance growth. This was a favorable result since it gave confidence that the emittance growth could be controlled by altering external fields.

We examined ways of optimizing the design to reduce the emittance growth. Decreas-

ing the size of the envelope by changing the focusing was simple but of limited help. The most effective way of reducing the emittance growth was to increase the beam energy from the source. This decreased the size of the beam and directly reduced the energy effect.

3.2 Comparison with experiment

A scaled-down version of the injector was built at LBNL as a proof-of-principle experiment. WARP3d simulations were used as a guide in the design of the experiment. Excellent agreement was found between the experiment and simulation results. The beam's transverse size and velocities at the end of the injector agreed to within a few percent. Qualitatively, the phase space $(x - p_x, y - p_y)$ images looked the same, and both displayed the same distortions that result from the nonlinear fields. The amount of the resulting emittance growth also agreed within a few percent.

The final design of the full size ESQ injector was made with the help of WARP3d simulations. The results of the simulations showed that, for the diode voltage, a balance could be reached between the requirement of low emittance growth and voltage breakdown limits. The design diode voltage of 750 kV produced a beam with acceptably little emittance growth and did not cause breakdown problems.

The diode region was designed using EGUN W.Herrmannsfeldt[7]. It consists of a source, an extraction electrode, and the first quadrupole end plate. The extraction electrode, a large aperture ring in front of the source, is held at a constant voltage above the first quadrupole end plate. The voltage on the source is varied to control emission of the beam particles. The simulations of the experiment with WARP3d start from the ion source, using space-charge limited injection and include the full geometry of the diode region.

The construction of the full size injector has been completed and it has met and indeed exceeded its requirements. A series of measurements have been taken with varying diode and quadrupole voltages. The simulation results compared well with the experiment measurements. Two cases are presented. Figure 2 shows the trace spaces at the optimized design point. No "S"-shape is evident. The beam size and divergence angle agree to within a few percent. Figure 3 shows trace spaces that result from a diode voltage which is one and a half times higher than the optimized design point. Both the experiment and simulation show the same, significant "S"-shape.

3.3 Time-dependent behavior

The time-dependent behavior of the ESQ is being studied with WARP3d. The beam was emitted from the source using space-charge limited injection. The time profile of the voltage on the source obtained from the experiment was used in the simulation. It is initially held at a negative voltage to hold back the ions. It is ramped up to a positive voltage with a rise time of 0.5 μs, held for 1.5 μs, and ramped back down to a negative voltage with a fall time of 0.5 μs.

Figure 4 shows the comparison of the current profile at the end of the ESQ from simulation and experiment. The rise and fall times of the current agree reasonably well. The lack of agreement in the height of the current is due to the fact that the simulation did

not include the variation of the voltage on the extraction electrode and due to inaccuracies in the particle injection algorithm.

4. Induction Recirculator

A small scale recirculating induction accelerator is being built to study beam dynamics in a recirculating accelerator and to examine various engineering design issues. A.Friedman[8] J.Barnard[9] The accelerator was designed to have beam dimensionless parameters relevant to those of a driver. With a circumference of 14.4 m, there are 40 half lattice periods, each with a permanent magnetic quadrupole, an electric dipole, and an induction acceleration gap (except in the insertion/extraction region). A beam of singly charged potassium ions will be accelerated from 80 to 320 keV over 15 laps, at a current increasing from 0.2 to 0.8 Amps. With a low emittance, the beam behavior is space-charge dominated. As designed, the phase advance is initially depressed from 72° to 16°.

4.1 Electric Dipoles

To make the construction of the recirculator easier and less costly, electric dipole plates were chosen to bend the beam. The length of the plate is constrained by the amount of space available for focusing and bending the beam. The maximum length that would fit is roughly one and a half times the plate separation. Also, the ends of the plates are near the structure supporting the quadrupole magnets. With the height of the plates limited similarly, the plates are nearly square. As a result of the constraints, there are significant nonlinear fields produced by the dipole plates.

Analysis of the dipoles' effect on the behavior of the beam calls for self-consistent simulations which include both the fields produced by the plates and the self-fields of the beams. WARP3d was used to carry out the simulations. Figure 5 shows the layout of the half lattice periods as used in the simulations.

The dominant nonlinear component of the field from the dipole plates is the sextupole component, $\phi \propto r^3 \cos(3\theta)$. With flat plates, the sextupole rapidly alters the beam shape. After one quarter of a lap the transverse profile of the beam becomes markedly triangular. Ridges were added on the top and bottom of the plates to alter the sextupole component. Because the axial fringe fields introduce a significant sextupole, the ridges have to be made large enough to drive the sign of the sextupole in the center of the plates negative so that the average of the sextupole over the lattice period is minimized. Figure 6 shows the beam transverse profile after traveling through a lattice with dipole plates without ridges.

The transverse variation of the potential across the beam in the dipole and the fringe fields gives rise to a focusing effect. The resulting phase advances along the two transverse axes can differ by up to 10^o, with the phase advance in the vertical plane being generally less. The plates can be curved along the vertical axes to increase the vertical focusing. The radius of curvature needed is comparable to the radius of curvature of the accelerator.

The change in potential along the beam centroid in the dipole changes the speed of the beam in the dipole, changing the overall timing of the beam. If the resulting timing change is not included in the timing of the axially confining fields, significant line charge waves will be launched from the ends of the beam. The change in the timing can be

controlled by adjusting the radial location of the dipole plates, which changes the location of the potential in the beam relative to ground.

The plate shape has been tuned to minimize the effects described above. The design of the plates developed is shown in figure 7. The undepressed phase advances in both planes are near 79.5° with a phase advance with quadrupoles only of 72°. With a beam energy of 80 kV, the plates are held at ±7000 V. The design was arrived at by iteratively adjusting the curvature and ridges until the in-plane and out-of-plane focusing matched, and then adjusting the radial location of the plates to bring the timing change to zero.

4.2 Simulation Results

WARP3d is being used to simulate the beam in the recirculator for 15 laps. Typically, the beam, which is of order 3.5 half-lattice periods or 2 μs long, is made up of 100,000 simulation particles. The field grid has dimensions 32x16 in the transverse plane and 128 cells axially, covering four half lattice periods. The up-down symmetry is taken advantage of and only the top half of the accelerator is simulated, allowing the use of half the number of grid cells in the vertical direction. The quadrupoles are modeled as hard edged, with no nonlinear components. Subsidiary calculations with realistic quadrupoles showed only minor differences.

The tuned dipole plate shape described in the previous section is used in the simulations. The plates are modeled self-consistently except for image field effects. The field from the dipole plates is calculated with Laplace's equation with the successive overrelaxation (SOR) field solver, including the detailed shape of the plates and the surrounding conductors. During the simulation, the pre-calculated field of the dipole is overlaid on top of the beam self-fields. The self-fields are calculated with a 3-D FFT which is faster than the SOR solver. The FFT field solve is done in a rectangular box with the implicit image charges on the sides. The transverse dimensions of the box are the same as the plate separation. This only approximates the true images on the dipole plates and quadrupole pipe, but the images are small and the difference is negligible.

The accelerating schedule and axially confining fields give a beam with constant physical length. The accelerating field is ramped up linearly in time during the first lap. For the remaining laps, the field is held constant. The axially confining fields, which are not varied throughout the simulation, are continuously applied to the beam ends. The voltage on the dipole plates is scaled with the energy of the beam center.

The simulations show an initial increase in emittance on the order of 50% as the beam matches itself from a straight path to a curved path. This growth is due to a separation of the particles with differing axial velocities in the bends producing nonlinearities in the space charge. The nonlinearities thermalize, producing an increase in emittance. The amount of growth agrees with theoretical analysis J.Barnard[10].

After 15 laps, there was little further growth in the emittance. Figure 8 shows the time history of the x and y normalized emittances at the beam mid-pulse. The amount of emittance growth is well within acceptable limits. The small jump in emittance at the end of the simulation is numerical in origin.

In the experiment, pulse compression will be done to increase the line charge, and the transverse size of the beam will correspondingly grow. The simulations do not yet include

pulse compression. Two cases were therefore simulated, one with the transverse size of the simulated beam set to that of the physical beam as it enters the recirculator, and the other with it set to the larger size of the beam upon exit from the recirculator, after pulse compression. Figure 8 shows the results of the former case. The latter case has the same result, little emittance growth after the initial increase.

The rms beam size is affected by the focusing from the electric dipole plates. With permanent magnetic quadrupole focusing alone, an accelerating beam would show smaller alternating gradient flutter but the average of the beam size would not decrease. The dipole fields, though, vary with time: the voltage is increased proportionately with the beam energy to maintain the same bend angle. This also increases the focusing, causing the average beam transverse size to decrease.

5. Conclusions

WARP3d simulations have helped demonstrate the feasibility of two experimental accelerators. For the ESQ injector, the simulations helped in the understanding of the emittance growth and showed that it could be greatly reduced. The final design of the full size ESQ was made in part using WARP3d. The simulation results were used to find a balance between the requirements of low emittance growth and breakdown voltage limits. The injector met and exceeded its requirement to deliver a 0.8 MV beam at low normalized emittance (< 1 mm-mrad).

For the small induction recirculator experiment, WARP3d simulations showed that a beam could be propagated through 15 laps using electric dipole bending with minimal growth in transverse normalized emittance. There was little further emittance increase after the initial unavoidable increase due to matching to the bent lattice. Critical to the success was the design of the electric dipole plates. They were designed to minimize the effects of the nonlinear fields which result from the compact design of the dipole plates and half lattice period.

References

[1] A. Friedman, D. P. Grote, and I. Haber, Three-dimensional particle simulation of heavy-ion fusion beams, Phys.Fluids B 4 (1992), 2203.

[2] P. F. Dubois et. al., The Basis System, LLNL Document M-225 (1988).

[3] S. Yu, Heavy Ion Fusion Injector Program, Proceedings of the 1993 Particle Accelerator Conference, pp 703-705.

[4] S. Yu, et.al., these proceedings

[5] E. Henestroza, et.al., these proceedings

[6] E. Lee, et.al., these proceedings

[7] W. B. Herrmannsfeldt, EGUN-An Electron Optics and Gun Design Program, technical report 331, SLAC, 1988

[8] A. Friedman, et.al., these proceedings

[9] J. Barnard, et.al., these proceedings

[10] J. J. Barnard, H. D. Shay, S. S. Yu, A. Friedman, and D. P. Grote, Emittance growth in Heavy Ion Recirculators, 1992 Linear Accelerator Conference Proceedings, vol. 1,p 229, (1992)

Figure captions

1. The layout of the ESQ injector. Shown are the source, diode, quadrupoles, and insulating column surrounding the injector.

2. Comparison of trace spaces at the end of the ESQ injector with the diode voltage at the optimized design point. a) is the experimental measurement, b) is from the simulation.

3. Comparison of trace spaces at the end of the ESQ injector with the diode voltage 50% higher than the optimized design point. a) is the experimental measurement, b) is from the simulation.

4. Comparison of the profile of the current at the end of the ESQ from WARP3d simulation and the experiment. WARP3d produced a slightly lower current. The agreement is not exact partly because the variation of the voltage on the extraction electrode was not included in the simulation.

5. Top view of the geometry of the recirculator half lattice period as used in WARP3d.

6. Transverse beam profile after traveling through a lattice with dipole plates without ridges. The uncorrected sextupole component significantly distorts the beam, making it triangular. The deformation is rapid, occurring within 1/4 of a lap.
7. The optimized design of the dipole plate, minimizing emittance growth. The beam goes into the page and is bent to the left.

8. Time histories of the mid-pulse normalized emittance with the optimized design of the dipole plates a) in the plane of the bend and b) out of the plane of the bend. There is acceptably little growth after the initial increase which is due to the beam matching to the bent lattice.

David P. Grote
Figure 1

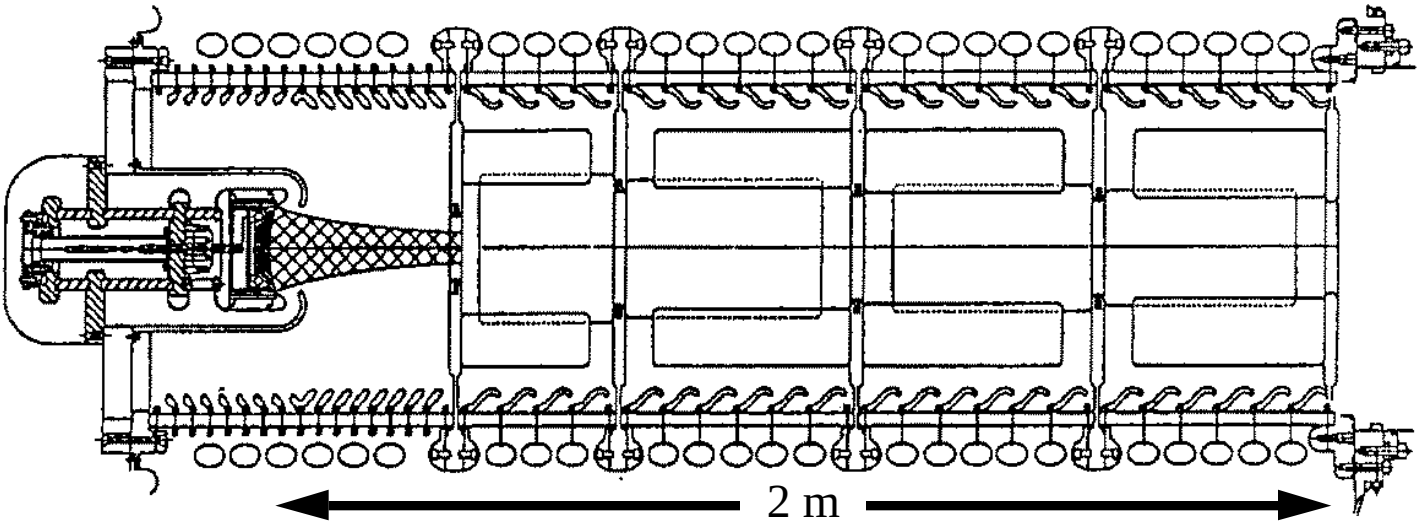

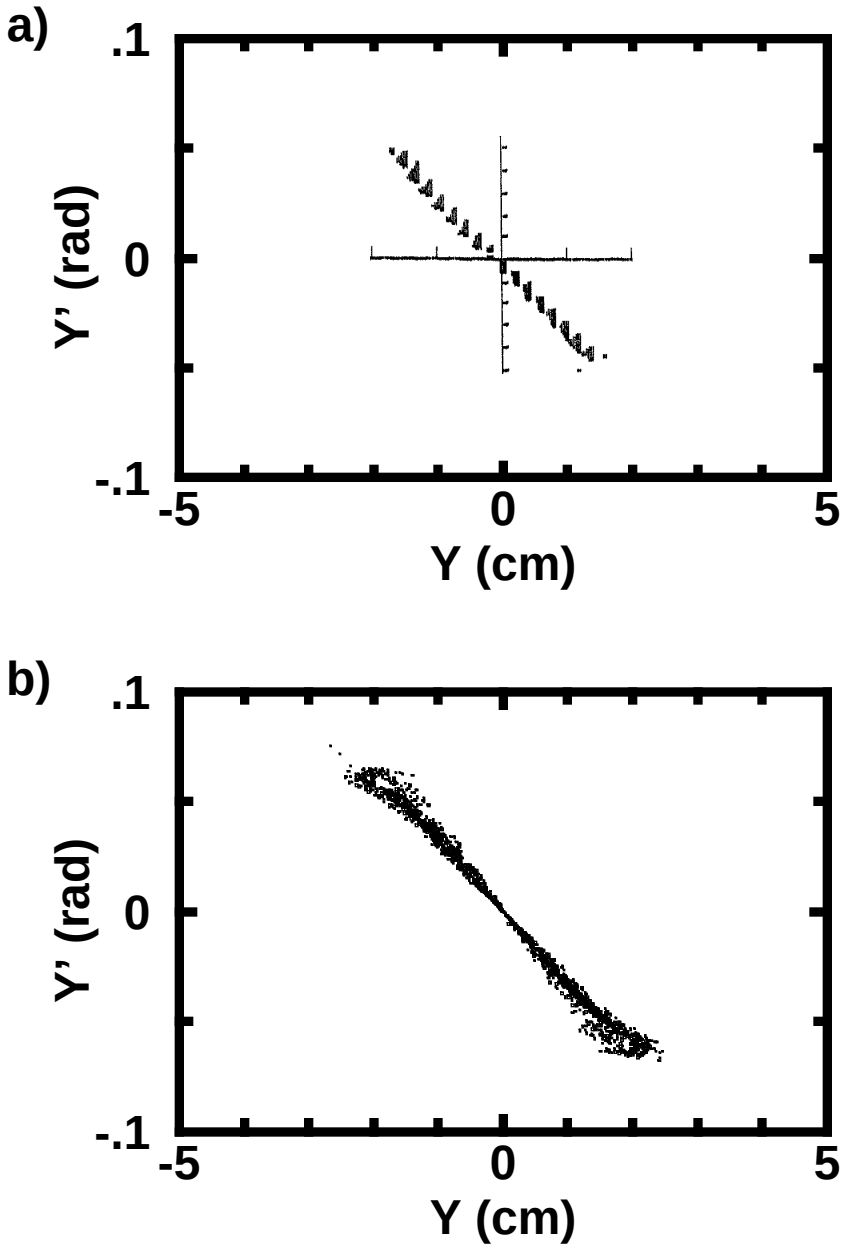
a)
.1
0
-.1
Y' (rad)
-5
0
5
Y (cm)
b)
.1
0
-.1
Y' (rad)
-5
0
5
Y (cm)

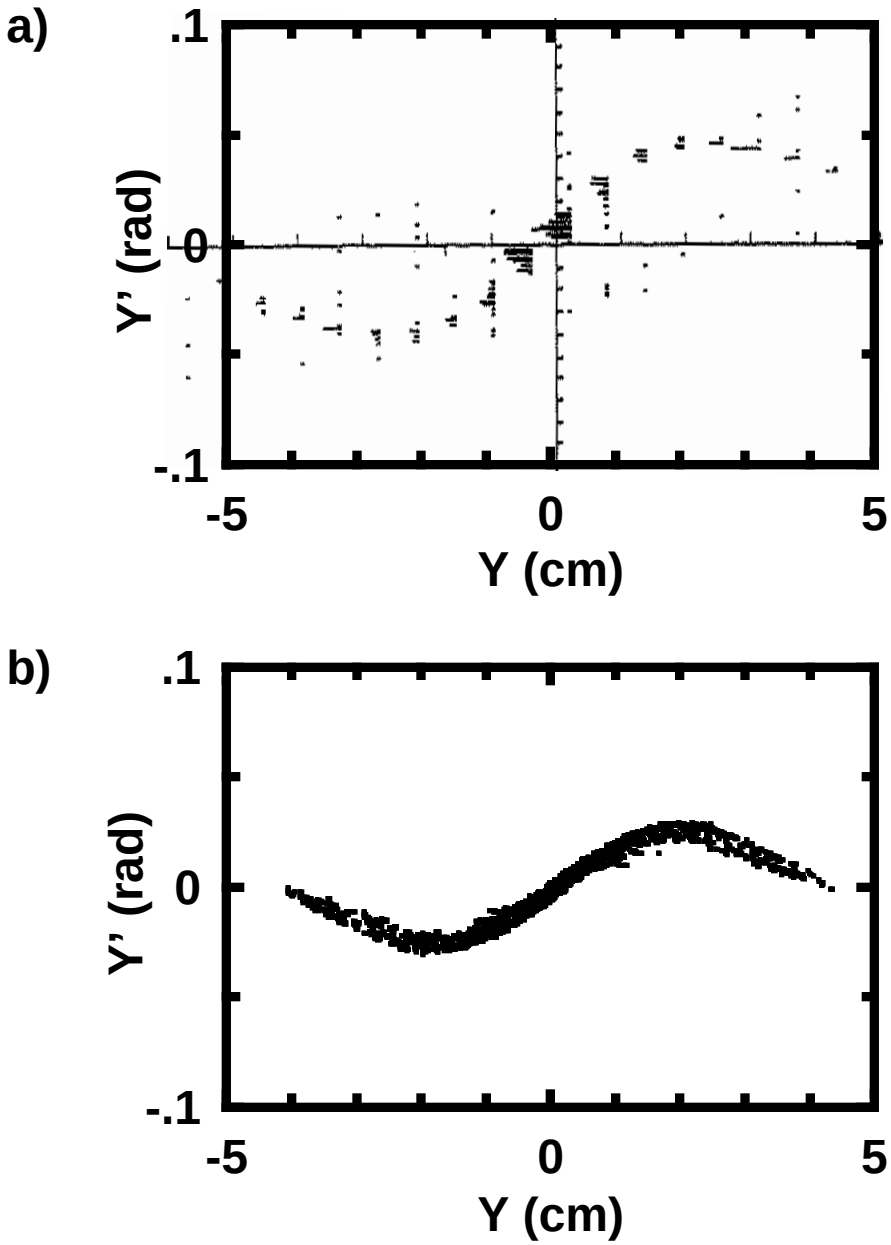
a)
.1
0
-.1
Y' (rad)
-5
0
5
Y (cm)
b)
.1
0
-.1
Y' (rad)
-5
0
5
Y (cm)

David P. Grote
Figure 4

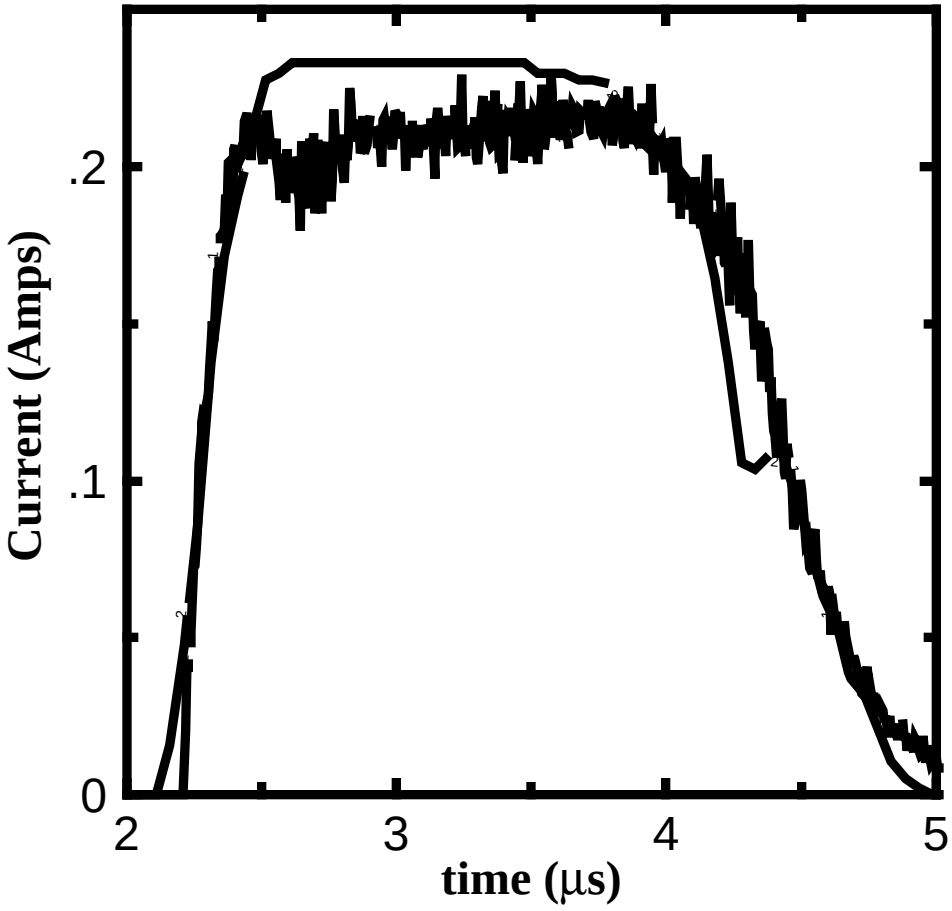

David P. Grote
Figure 5

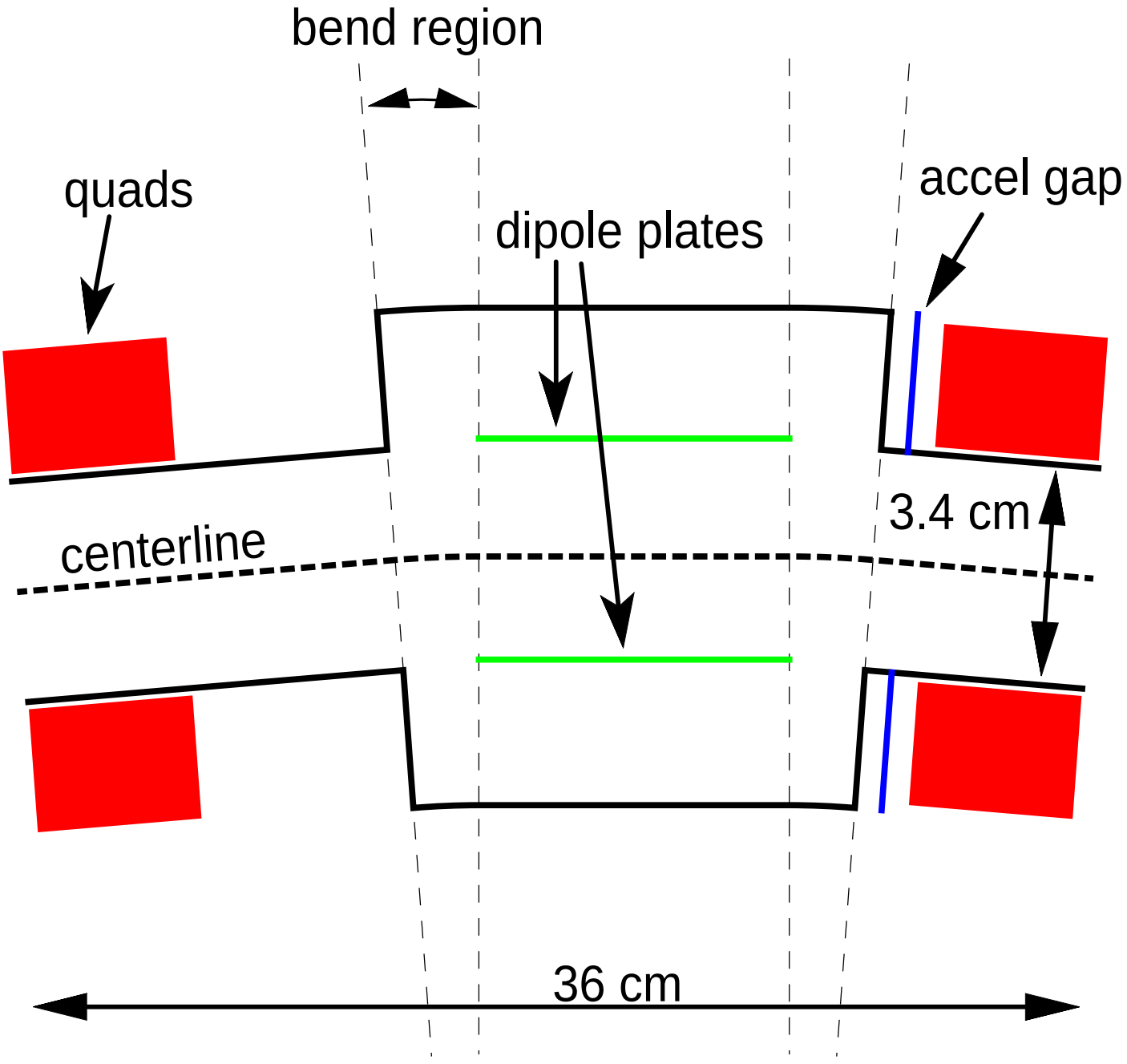

David P. Grote
Figure 6

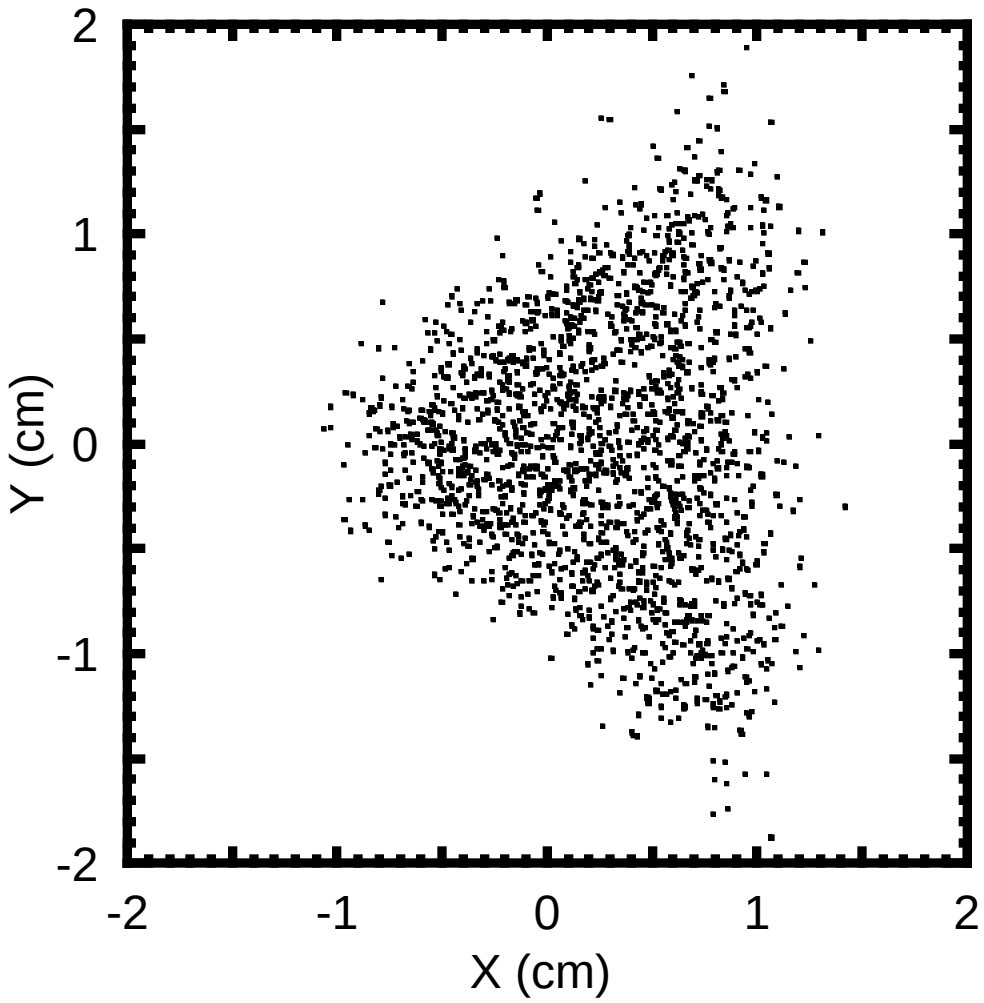

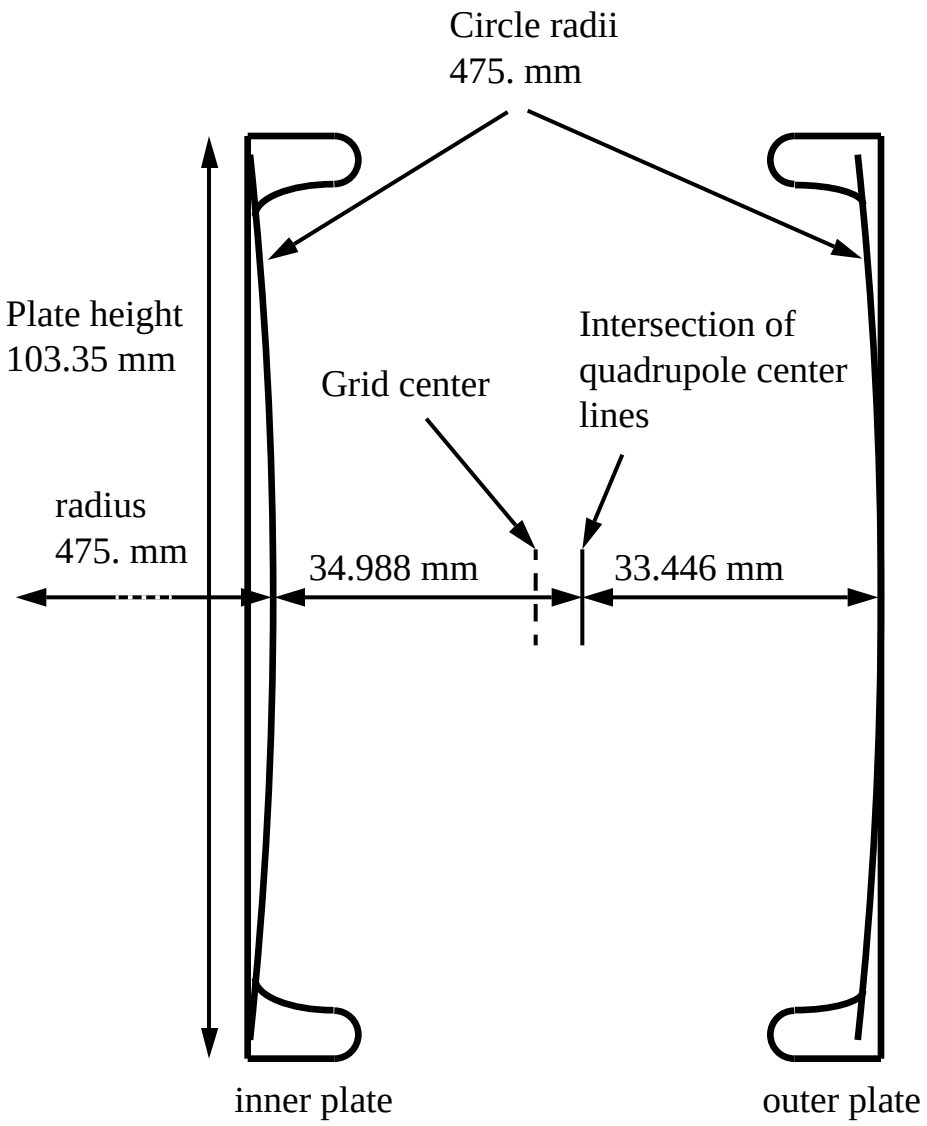
Circle radii
475. mm
Plate height
103.35 mm
Grid center
Intersection of
quadrupole center
lines
radius
475. mm
34.988 mm
33.446 mm
inner plate
outer plate

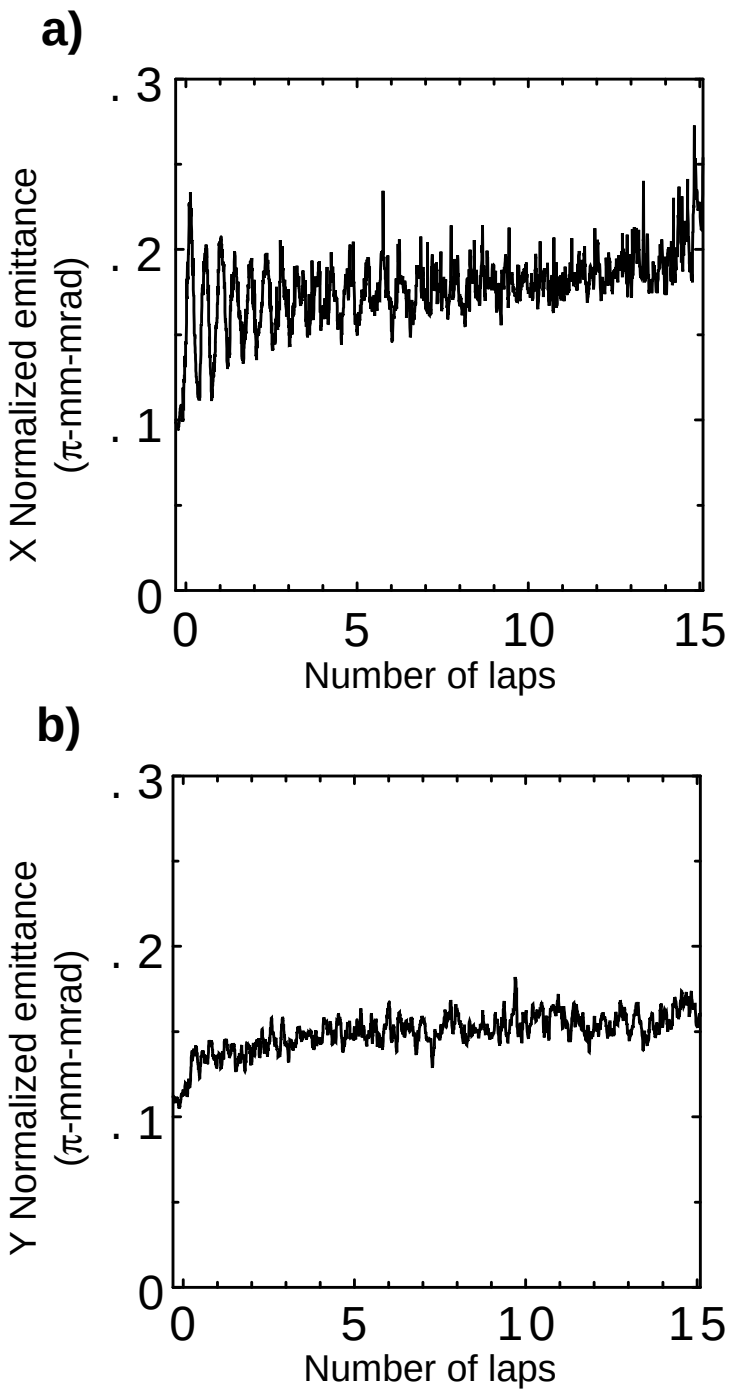
a)
X Normalized emittance
(π-mm-mrad)
.3
.2
.1
0
0
5
10
15
Number of laps
b)
Y Normalized emittance
(π-mm-mrad)
.3
.2
.1
0
0
5
10
15
Number of laps